THE JOURNAL OF PHYSICAL CHEMISTRY B

Article

pubs.acs.org/JPCB

# Effect of Hierarchical Cluster Formation on the Viscosity of Concentrated Monoclonal Antibody Formulations Studied by Neutron Scattering

P. Douglas Godfrin,[†] Isidro E. Zarraga,[*,‡] Jonathan Zarzar,[‡] Lionel Porcar,[§] Peter Falus,[§] Norman J. Wagner,[†] and Yun Liu[*,†,∥]

[†]Department of Chemical and Biomolecular Engineering, University of Delaware, Newark, Delaware 19716, United States

[‡]Late Stage Pharmaceutical Development, Genentech Inc., South San Francisco, California 94080, United States

[§]Institut Laue-Langevin, 71 Avenue des Martyrs, CS 20156, 38042 Grenoble Cedex 9, France

[∥]Center for Neutron Research, National Institute of Standards and Technology, Gaithersburg, Maryland 20899, United States

Supporting Information

**ABSTRACT:** Recently, reversible cluster formation was identified as an underlying cause of anomalously large solution viscosities observed in some concentrated monoclonal antibody (mAb) formulations, which poses a major challenge to the use of subcutaneous injection for some mAbs. A fundamental understanding of the structural and dynamic origins of high viscosities in concentrated mAb solutions is thus of significant relevance to mAb applications in human health care, as well as being of scientific interest. Herein, we present a detailed investigation of an IgG1-based mAb to relate the short-time dynamics and microstructure to significant viscosity changes over a range of pharmaceutically relevant physiochemical conditions. The combination of light scattering, small-angle neutron scattering, and neutron spin echo measurement techniques conclusively demonstrates that, upon addition of $Na_2SO_4$, these antibodies form strongly bound reversible dimers at dilute concentrations that interact with each other to form large, loosely bound, transient clusters when concentrated. This hierarchical structure formation in solution causes a significant increase in the solution viscosity.

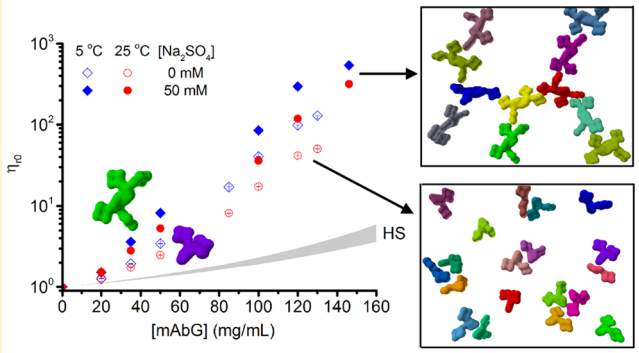


## INTRODUCTION

The successful commercialization of biopharmaceutical therapeutic products is facilitated by understanding the relationship between protein structure and solution properties, such as stability and viscosity, in addition to the biological functionality. A significant challenge in biopharmaceutical development is maintaining bioefficacy from production through storage and delivery.[1−4] Depending on the solution physicochemical conditions (pH, temperature, ionic strength, electrolyte valency, etc.) and protein composition/structure, proteins can partially unfold and irreversibly aggregate or reversibly associate with each other while maintaining their native structure.[5] Whereas the former impacts product impurity and potentially potency,[6,7] the latter can have strong effects on manufacturability and product delivery.[8,9]

Monoclonal antibodies (mAbs) have become the most rapidly growing sector of the biopharmaceutical market in large part because of their specific interactions dictated by the complementarity-determining region (CDR) and good safety profile. It has been demonstrated that some mAbs in solution under specific physiochemical conditions can form small reversible clusters and exhibit a dramatic increase in solution viscosity with increasing concentration and/or decreasing temperature.[10−15] Relatively small deviations in the primary sequence can cause an order-of-magnitude difference in solution viscosity at elevated concentrations.[10,11,16] As a result, biologically unimportant changes in protein primary sequence can significantly affect the ability to produce and deliver these mAbs as a therapeutic product.[9]

Reversible cluster formation has been intensively studied in colloidal suspensions[17−21] and solutions of globular proteins such as lysozyme,[22,23] where the interaction contains both a short-range attraction and long-range repulsion. Globular proteins are often used as model systems to test models developed for colloidal suspensions because of their stable tertiary structures and effective interactions that can often be modeled, to first order, as spherically symmetric.[23−26] The short-range attractions drive association into clusters, but the

**Received:** July 27, 2015
**Revised:** November 19, 2015
**Published:** December 27, 2015





DOI: 10.1021/acs.jpcb.5b07260
J. Phys. Chem. B 2016, 120, 278−291

association to a cluster surface is eventually limited by the overall charge of a cluster, leading to greater long-range repulsion between clusters (or between a cluster and a protein in solution). The attractive and repulsive interactions capable of forming clusters and their subsequent anisotropic shape are known to increase the solution viscosity.[27,28]

Solutions of mAbs are challenging to study at high concentrations because of highly nonspherical shape and heterogeneous charge distribution on the mAb surface.[12,14,15,29]

Recent work has shown that a type of reversible cluster formation is the underlying source of the anomalous large viscosity observed at high protein concentrations.[14,15] In these solutions, at very low electrolyte concentrations, the formation of small, long-lived, elongated clusters is driven by an anisotropic electrostatic attraction between mAbs. These clusters are the driving force of a significantly high solution viscosity.[15] Adding large amounts of electrolyte significantly weakens the anisotropic attraction, which reduces the number of clusters and results in a significant decrease of the viscosity.

In this work, we study an IgG1 monoclonal antibody that was the subject of earlier research showing complex solution behavior as a function of protein concentration, ionic strength, and temperature.[13] Of particular relevance here, Lilyestrom et al. showed that this mAb has both compact and elongated monomer structures at very low concentrations.[30] Importantly, this previous research demonstrates that the tertiary conformation of IgG1 does not change with variations in temperature and added $Na_2SO_4$ concentration such as those studied here.[30] In further work, the same researchers demonstrated that, in the presence of $Na_2SO_4$, these proteins can form extended dimers at relatively low concentrations.[13] Furthermore, reversible cluster formation was observed with increasing mAb concentration as derived from modeling of static light scattering results.[13,31] The authors concluded that the viscosities of dilute and semidilute mAb solutions correlate linearly with the equilibrium cluster size.[13] However, important questions remain about the structure of the clusters in concentrated solutions, the dynamic exchange of proteins into and out of these clusters, and the quantitative relationship between these dynamic clusters and the solution rheology.

Methods to address these questions on the nanoscale have been demonstrated in our group by combining neutron spin echo, small-angle neutron scattering, dynamic light scattering, and rheology measurements. Previous research using these methods has shown both similarities and differences in the behaviors of concentrated solutions of several monoclonal antibodies. In particular, the behavior of the mAb in this work with added electrolyte was found to be opposite to that reported previously for a different IgG1 mAb. Specifically, whereas adding electrolyte significantly decreased the solution viscosity in the previous case, the added electrolyte increased the viscosity dramatically for the mAb investigated here.[14,15]

Despite the apparent differences in controlling the solution viscosity, we show that the underlying physical mechanism driving the high viscosity in concentrated mAb solutions is similar for both mAbs in solution—namely, the increase in viscosity is due to the formation of reversible protein clusters. The interprotein microstructure was found to be even more complex in the current study. Using neutron scattering techniques, the addition of electrolyte was found to promote the formation of small clusters that persist to high concentration. Importantly, the small, strongly bound clusters interact with each other to form loosely bound transient networks, as probed by rheology. This hierarchical structuring of clusters significantly increases the viscosity of the concentrated protein solutions. In addition, we have tried to qualitatively understand the interactions between our proteins using neutron scattering data to illustrate the driving force for this hierarchical cluster formation in our protein solutions.

This article is organized as follows: The Theories and Experimental Methods section describes the experimental methods used, together with the necessary theories required to analyze the data obtained from different experimental methods. The Results and Discussion section consists of several subsections explaining all of our observations and conclusions. It starts with the viscosity data as functions of protein concentration and salt conditions. Then, we discuss the solution protein structure in the dilute and concentrated cases as determined by neutron spin echo spectroscopy and dynamic light scattering. We then present the rheological data, from which we semiquantitatively extract a structural length scale used to construct a comprehensive understanding of the solution protein structure. We further analyze our small-angle neutron scattering data to qualitatively obtain the effective protein−protein interaction and its impact on the solution protein structure. This section ends with a discussion of relating the solution properties to the viscosity using different theoretical and empirical models. The major findings are then summarized in the Conclusions section.

## THEORIES AND EXPERIMENTAL METHODS

**Materials.** The monoclonal antibody examined in this study is a humanized IgG1 protein produced by Genentech, Inc., referred to herein as mAbG. Importantly, mAbG as it is labeled here is the same antibody reported in previous publications.[13,30] The protein was expressed in Chinese hamster ovarian (CHO) cells and subsequently purified by multiple chromatographic methods including ion-exchange chromatography. The antibody was then dialyzed into a buffer composed of 20 mM L-histidine hydrochloride (His-Cl) in deuterium oxide ($D_2O$ or heavy water) at pH 6.0 with 0.02 wt % polysorbate-20 surfactant and two concentrations of $Na_2SO_4$ electrolyte (0 and 50 mM). For reference, a 50 mM solution of $Na_2SO_4$ has an ionic strength of 0.15 M and would theoretically produce a Debye screening length of about 0.78 nm. A stock solution with an mAbG concentration of 150 mg/mL was obtained using tangential flow filtration and diluted for all concentrations studied. All samples were stored at 4 °C between production and experimentation. Samples with 50 mM $Na_2SO_4$ were formulated by adding the required amount of 1 M $Na_2SO_4$ buffer solution to an electrolyte-free stock protein solution.

**Small-Angle Neutron Scattering (SANS).** Experiments were conducted on the D-22 and D-33 beamlines at the Institut Laue-Langevin (ILL) in Grenoble, France, as well as at the NG-B 30-m SANS instrument at the NIST Center for Neutron Research (NCNR) in Gaithersburg, MD, USA, following previously reported protocols and methods.[14,15,22] The scattering intensity was obtained over scattering vector magnitudes ($q$) ranging from 0.003 to 0.53 $Å^{-1}$. All samples were held in standard quartz Hellma cells at ILL and custom titanium cells with quartz windows at NCNR. Low-concentration samples were studied using cells with a 2-mm path length to enhance intensity, whereas concentrated samples were studied in cells with a 1-mm path length. A range of mAb concentrations was studied at two temperatures (5 and 25 °C).


DOI: 10.1021/acs.jpcb.5b07260
J. Phys. Chem. B 2016, 120, 278−291

The coherent scattering intensity from a solution of (slightly) nonspherically symmetric particles such as mAbs, for which the intra- and interparticle correlations are weakly coupled, is represented by[32,33]

$$I(q) = \phi V(\Delta\rho)^2 P(q)\{1 + \beta(q)[S(q) - 1]\} \quad (1)$$

where $q = (4\pi/\lambda)\sin(\theta/2)$, $\lambda$ is the neutron wavelength, $\theta$ is the scattering angle, $\phi$ is the particle volume fraction, $V$ is the volume of one individual particle, and $\Delta\rho$ is the scattering length density (SLD) difference between the particle and solvent. $P(q)$ is the normalized particle form factor, which is the Fourier transformation of the intraparticle density correlations. The interparticle structure factor, $S(q)$, is related to the Fourier transformation of the pair distribution function (i.e., the correlation of the centers of mass of all particles in solution).[34] The term in braces in eq 1 is the effective structure factor, $S_{eff}(q)$, which is related to the true structure factor, $S(q)$, through the decoupling function, $\beta(q)$, a $q$-dependent function of the protein shape.

At dilute concentrations, where $S_{eff}(q) \approx 1$, the ensemble-average radius of gyration, $R_g$, and molecular weight, $M_w$, can be calculated in the limit of very small $q$ values. The Guinier approximation enables the determination of $R_g$ from the slope of the natural logarithm of the scattering intensity by expanding the Fourier transform of intraparticle density correlations with the first term in the McLaurin series in the limit of small $q$ values, resulting in the expression

$$\ln[I(q)] = \ln[I(0)] - (qR_g)^2/3 \quad (2)$$

The Guinier analysis is applicable within a $q$ range of $q < 1.0/R_g$ and is limited to solutions of noninteracting scattering entities [i.e., $S(q) \approx 1$]. The extracted value of $I(0)$ can be used to estimate the molecular mass of a protein or protein cluster, which is expressed as

$$I(0) = NV^2(\Delta\rho)^2 = \frac{N_A C v_0^2 (\Delta\rho)^2}{M_w} \quad (3)$$

where $N_A$ is Avogadro's constant, $C$ is the protein mass concentration, and $v_0$ is the specific volume of the mAb, again assuming that the system is noninteracting [i.e., $S(0) \approx 1$]. However, as the concentration is increased, interactions will make a significant contribution to scattering at low $q$ values [i.e., $S(q) \neq 1$]. Therefore, the molecular weight extracted from such an analysis will be an apparent molecular weight, $M_{w,app}$, similarly to that obtained by static light scattering.[13,31]

To quantitatively study the shape of an mAb protein, a 12-bead model of mAb structure is described in detail in the Supporting Information (SI). This model allows the structure of the shape of one mAb particle and the formed dimer to be extracted reasonably accurately. Here, we use a 2 mg/mL sample under each solution condition studied to determine $P(q)$, where $S_{eff}(q) \approx 1$. By minimizing the residual between the data and model, the most representative protein conformation can be observed in real-space coordinates. For the purposes of this study, the model is sufficiently sensitive to the conformation of the beads to distinguish between compact and elongated structures (for additional details, see the SI).

We further investigate the interprotein interaction by modeling $S_{eff}(q)$ and calculating $\beta(q)$ using our 12-bead model.[35] Using integral equation theory, $S(q)$ can be directly related to the parameters of an effective interaction potential for a system with an isotropic interaction.[36] We recognize that mAb proteins have anisotropic interactions and, therefore, the true interaction potential will not be spherically symmetric. However, as a first approximation, the anisotropic mAb−mAb interactions can be modeled using an isotropic interaction potential to study effective interactions across various solution conditions. Previous studies have successfully represented globular protein interactions by a combination of attractive and repulsive forces.[23,25,37] Therefore, we fit the data with a structure factor derived from a potential that combines a hard-sphere excluded volume with a double Yukawa potential (HSDY), which is expressed as

$$\frac{U(r)}{kT} = \begin{cases} \infty & r < 1 \\ \frac{1}{r}[-K_1 e^{-z_1(r-1)} + K_2 e^{-z_2(r-1)}] & r \geq 1 \end{cases} \quad (4)$$

In eq 4, $r$ is the center-to-center separation normalized by the effective diameter of the protein determined by fitting the SANS data. $K_1$ and $K_2$ are the strengths of the short-range attraction and long-range repulsion, respectively, and $z_1$ and $z_2$ are the normalized ranges of attraction and repulsion, respectively. The structure factor is calculated for the HSDY potential using the Ornstein−Zernike equation and a thermodynamically self-consistent closure relation developed previously.[38] In our case, the region of small $q$ values ($q < 0.07$ Å$^{-1}$) is more sensitive to the details of interparticle interactions that lead to longer-range structural features.

**Neutron Spin Echo (NSE) Spectroscopy.** Experiments were performed on the IN-15 beamline at ILL in Grenoble, France. Samples were prepared on site, pipetted into 1-mm square quartz cells, and stored in a custom temperature-controlled sample chamber. All samples were allowed 30−60 min to reach thermal equilibrium at each of the temperatures studied. Intermediate scattering functions (ISFs), represented as $I(q,t)$, were obtained with the correlation time up to 50 ns at 30−35 $q$-value points ranging from 0.03 to 0.20 Å$^{-1}$ at each set of sample conditions studied.

NSE spectroscopy is a powerful technique, capable of observing short-time dynamics with high resolution over a range of length scales. Typically, for a colloidal system, different time scales are associated with different types of dynamics. If we denote $\tau_B$ as the momentum relaxation time and $\tau_I = R_g^2/D_0$ as the structural relaxation or interaction time, the time scale of short-time dynamics is within the range $\tau_B \ll t \ll \tau_I$.[39] Based on the protein's size ($R_g \approx 5$ nm) and self-diffusivity ($D_0 \approx 37$ $\mu$m$^2$/s at 25 °C), the NSE correlation times explored here probe the short-time diffusion of mAbG. Specifically, "short" length scales refer to roughly 10 nm, or the size of the protein, and "short" time scales extend up to about 50 ns, much smaller than $\tau_I$.

In the short-time limit, the ISF can be fit with a single exponential function to extract a $q$-dependent collective diffusion coefficient, $D_c(q)$, according to

$$\frac{I(q,t)}{I(q,0)} = A\exp[-q^2 D_c(q)t] \quad (5a)$$

$$D_c(q) = D_0[H(q)/S(q)] \quad (5b)$$

where $D_0$ is the free diffusion coefficient, representing particle mobility in the infinitely dilute limit.[39,40] The hydrodynamic function, $H(q)$, represents the effect of hydrodynamic interactions due to the flow of solvent molecules generated by particle motion. $H(q)$ can be decomposed into a $q$-


DOI: 10.1021/acs.jpcb.5b07260
J. Phys. Chem. B 2016, 120, 278−291

independent term, $D_s/D_0$, the short-time self-diffusion coefficient, and a distinct hydrodynamic function, $H_d[q;S(q)]$, which is a function of the solution structure factor and therefore particle interactions. In the limit of large $q$ values, $S(q)$ approaches a value of 1, and $\lim_{q\to\infty}H(q) = D_s/D_0$, leading to $\lim_{q\to\infty}D_c(q) = D_s$.[22,41] Therefore, the short-time self-diffusion of mAbG can be extracted from the high-$q$-value limit of NSE data.

**Dynamic Light Scattering (DLS).** A DynaPro NanoStar instrument (Wyatt Technology Corp., Santa Barbara, CA)[42] was used for dynamic light scattering (DLS) measurements of mAb formulations over a range of concentrations and temperatures. All samples were allowed to thermally equilibrate at each temperature for 30 min before five independent measurements of the scattered intensity were recorded. The instrument was operated with a 663-nm-wavelength laser at a 90° scattering angle. The scattering wave vector was calculated according to $q = (4\pi n/\lambda)\sin(\theta/2)$, where $n$ is the refractive index of the sample determined by $n = n_s + c_{mAb}(dn/dc)$. The solvent refractive index, $n_s$, was assumed to be equal to that of pure $D_2O$ (1.328), and $dn/dc = 0.185$ mL/g. The $q$ values are roughly 0.0018 $Å^{-1}$, which is representative of "long" length scales on the order of 350 nm, and the DLS correlation time extends to "long" time scales on the order of milliseconds.

All DLS data were analyzed using the standard relation between the correlator output function and the autocorrelation function.[43] In the limit of high protein concentration, multiple relaxation modes can exist in solution, which is revealed by a nonlinear slope when plotting the ISF as a function of time on a semilogarithmic plot. The dynamics in mAb solutions appears to transition from a single relaxation mode to two modes with increasing concentration. Therefore, the ISF is modeled using a double-exponential decay, which extracts a primary relaxation mode, $D_{c,1}(q)$, and secondary relaxation mode, $D_{c,2}(q)$, according to

$$\frac{I(q,t)}{I(q,0)} = A_1\exp[-q^2D_{c,1}(q)t] + A_2\exp[-q^2D_{c,2}(q)t] \quad (6)$$

At low concentration, the effective hydrodynamic radius, $R_h$, can then be estimated according to the Stokes–Einstein–Sutherland relation: $R_h = kT/(6\pi\eta_s D_{c,1})$, where $\eta_s$ is the solvent viscosity and $k$ is the Boltzmann constant.

**Rheology.** The solution viscosity, $\eta$, of each mAb sample was obtained using an Anton Paar MCR-301 rheometer[42] with a titanium cone (50 mm, 0.3°), which required a sample volume of 175 μL. Each sample was allowed to equilibrate at each temperature for 20 min, during which a solvent trap was used to minimize solvent evaporation. Steady shear measurements were made by ramping the shear rate, $\dot{\gamma}$, from 10 to 10000 $s^{-1}$ and back down to check for reversibility. The viscosity at each shear rate was determined from the average stress measured over a given time window, which followed the logarithmic shift in shear rate from 30 to 5 s. Zero-shear viscosity was calculated as the average value of the data points within the plateau region at low shear rate. The upper limit of this region varied from 200 $s^{-1}$ at the highest concentrations to 1000 $s^{-1}$ at low concentrations. The reduced zero-shear viscosity, $\eta_{r0} = \eta/\eta_s$, was calculated by normalizing the solution viscosity by the solvent viscosity at the same temperature with the same electrolyte concentration.

Samples with 50 mM $Na_2SO_4$ at 5 °C showed hysteresis during the ramp up and back down over the full range of shear rates. To resolve the issue, these samples required a short (3-min) preshear step at 1000 $s^{-1}$ before the ramp was performed from low to high shear rate. The shear-rate dependence measured by this method was reproducible in both ramp directions without hysteresis.

## RESULTS AND DISCUSSION

Measurements of the reduced zero-shear viscosity of mAbG are summarized in Figure 1 as a function of protein concentration

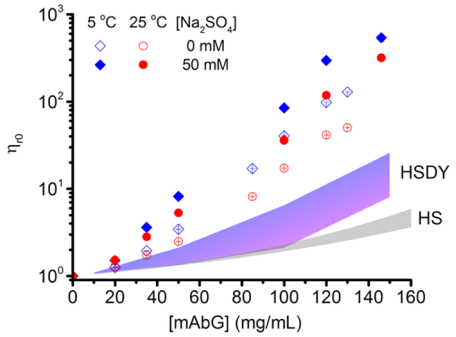


**Figure 1.** Reduced zero-shear viscosity (symbols) for all conditions of mAbG concentration, temperature, and electrolyte content studied. The experimental results are compared with estimates of hard-sphere dispersions (HS, gray region) and interacting protein solutions calculated using the hard-sphere double Yukawa potential with parameters from NSE and SANS data (HSDY, blue-red region). The ranges reflect differences in effective hydrodynamic radii and interaction parameters as a function of solution conditions. The upper (blue) portion of the HSDY range reflects low-temperature samples, whereas the lower (red) HSDY estimates represent higher temperatures.

for the four sets of solution conditions studied. Not surprisingly, a distinctive, strong increase in viscosity is observed with increasing protein concentration for all formulation conditions. However, samples at higher ionic strength have consistently exhibited higher viscosities. Further, lowering the temperature results in the solution viscosity increasing in excess of the buffer viscosity temperature dependence.

It is of great interest to identify the underlying microscopic structure and forces leading to the different macroscopic viscosities shown in Figure 1. For example, the choice of buffer dictates which formulations meet "syringeability" criteria at elevated protein concentrations, typically requiring viscosities much below 50 mPa·s.[8] Temperature and electrolyte have a measurable effect on the solution viscosity for protein concentrations as low as 35 mg/mL. By 120 mg/mL, the formulation with the lowest (0 mM $Na_2SO_4$ at 25 °C) and highest (50 mM $Na_2SO_4$ at 5 °C) viscosities differ by nearly an order of magnitude. The change in viscosity is influenced by both increasing ionic strength and reducing temperature, which are known to affect the net attractive strength between proteins.[44] Adding 50 mM $Na_2SO_4$ screens electrostatic repulsion between individual antibody molecules, potentially allowing attraction-induced association to become more prevalent. Further, decreasing the temperature can enhance the formation of large clusters induced by stronger short-range attractive interactions as observed in lysozyme solutions.[24] The viscosity of mAb solutions can also be estimated using different


DOI: 10.1021/acs.jpcb.5b07260
J. Phys. Chem. B 2016, 120, 278–291

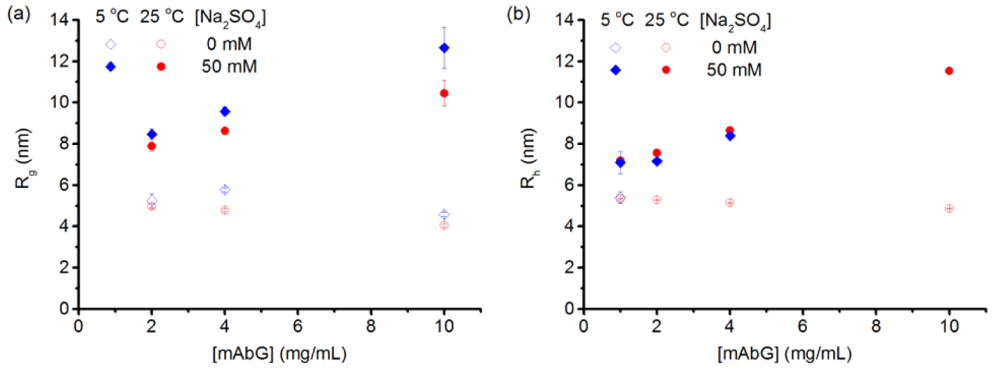


**Figure 2.** Comparison of (a) $R_g$ values extracted from Guinier analysis of low-concentration SANS data and (b) $R_h$ values estimated from DLS data using the Stokes−Einstein−Sutherland relation for mAbG samples with (open symbols) 0 and (solid symbols) 50 mM added electrolyte at (blue) 5 and (red) 25 °C.

interaction potentials (HSDY or HS). The results are shown in Figure 1, but will be discussed later in the article.

In the following, we first study the underlying building blocks of solution protein structures at low concentration to clarify the mechanism behind their assembly.

**Microstructure of Low-Protein-Concentration Solutions.** SANS data were obtained at 2 and 4 mg/mL with and without $Na_2SO_4$. The scattering patterns of mAbG solutions at low protein concentrations (10 mg/mL) with 0 and 50 mM added $Na_2SO_4$ were found to be different. In particular, the intensity at low $q$ values for samples with 50 mM electrolyte was roughly twice that of mAbG samples without electrolyte. Surprisingly, this difference in low-$q$ intensity, and other parameters, between samples with 0 and 50 mM electrolyte persisted to even lower protein concentrations.

Radii of gyration, $R_g$, are determined from a Guinier analysis of SANS data that is model-independent,[34] and hydrodynamic radii, $R_h$, are determined from independent DLS experiments at low concentrations. The results of these analyses are presented in Figure 2a and 2b, respectively. For samples with 0 mM $Na_2SO_4$, both radius values are almost independent of concentration and temperature. Without addition of electrolyte, $R_g$ and $R_h$ are roughly 5.0 and 5.3 nm, respectively, indicating that mAbG exists as monomers with little change up to 10 mg/mL. However, addition of 50 mM $Na_2SO_4$ to mAbG solutions (at 2 mg/mL) causes the effective radius of mAbG to increase by a factor of 1.4 relative to its size in solutions without electrolyte, as indicated by measurements of both $R_g$ and $R_h$. This increase is nearly identical to that reported in a previous study of a dimerizing mAb.[15]

Apparent molecular weights, extracted from SANS data and reported in Table 1, also indicate that the molecular mass is almost the same as that of a dimer in solution, even for samples as dilute as 2 mg/mL. This indicates that adding electrolyte causes mAbG to form dimers at very low concentrations, which are even lower than reported previously for mAb systems.[13,15,31] These results are also consistent with previous studies of mAbG in $H_2O$ buffers in the presence of $Na_2SO_4$.[13,30]

A more detailed modeling of SANS data can reveal the structure of the mAbG dimers in solutions with 50 mM $Na_2SO_4$. To estimate the real-space conformation of mAbG, we developed a new coarse-grained model to quantitatively determine the monomer and dimer structures and replicate the theoretical estimate of the antibody's neutron SLD. This 12-bead mAb model is presented and discussed in the SI, and only the optimal fits are shown here. The SANS data for a 2 mg/mL mAbG sample with 0 and 50 mM $Na_2SO_4$ are displayed in Figure 3, along with the best fits obtained using the model and the resulting real-space structures. The model fits the data remarkably well despite the fact that the scattering is a result of an ensemble average of antibody configurations.[45] Note that the data are multiplied by a constant value so that the fitting results from both samples can be clearly seen at high $q$.

**Table 1. Apparent Molecular Weights of mAbG Solutions at Low Concentrations with 0 and 50 mM Added Electrolyte at 25 and 5 °C**

| | | 25 °C | | 5 °C | |
|---|---|---|---|---|---|
| [mAbG] (mg/mL) | [$Na_2SO_4$] (mM) | $M_{w,app}$ (kDa) | $\sigma$ | $M_{w,app}$ (kDa) | $\sigma$ |
| 2 | 0 | 150.0 | 1.39 | 162.1 | 2.84 |
| 4 | 0 | 134.1 | 0.71 | 161.1 | 1.40 |
| 2 | 50 | 299.1 | 3.75 | 324.4 | 4.65 |
| 4 | 50 | 355.0 | 2.74 | 393.6 | 4.23 |

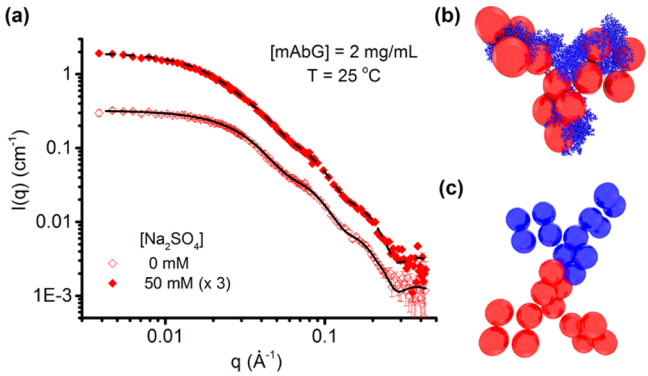


**Figure 3.** (a) SANS spectra of low-concentration (2 mg/mL) mAbG samples with (open symbols) 0 and (solid symbols) 50 mM added $Na_2SO_4$, along with best fits (lines) obtained using the coarse-grained model developed in the SI. The data with $Na_2SO_4$ are shifted by a constant value on the logarithmic scale to show the fitting result more clearly at high $q$. The most representative structures were determined to be (b) a monomer for samples without electrolyte (red), which is compared to the crystal structure of an IgG1 protein (blue), and (c) a dimer for samples with added electrolyte, where the two monomers are in different colors.



DOI: 10.1021/acs.jpcb.5b07260
J. Phys. Chem. B 2016, 120, 278−291

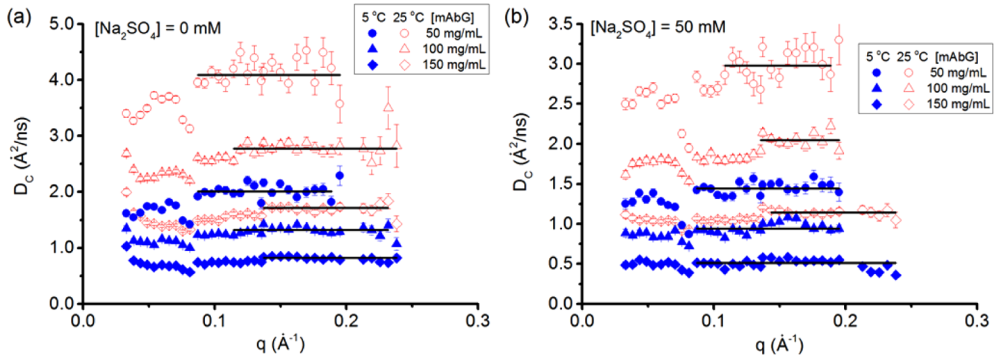


**Figure 4.** Collective diffusion coefficients extracted from fits to the NSE data as a function of $q$ value for samples with (a) 0 and (b) 50 mM added $Na_2SO_4$. The coefficients approach an asymptotic value in the limit of large $q$ values (lines), the average value of which (lines) indicates the short-time self-diffusion coefficient under each set of conditions.

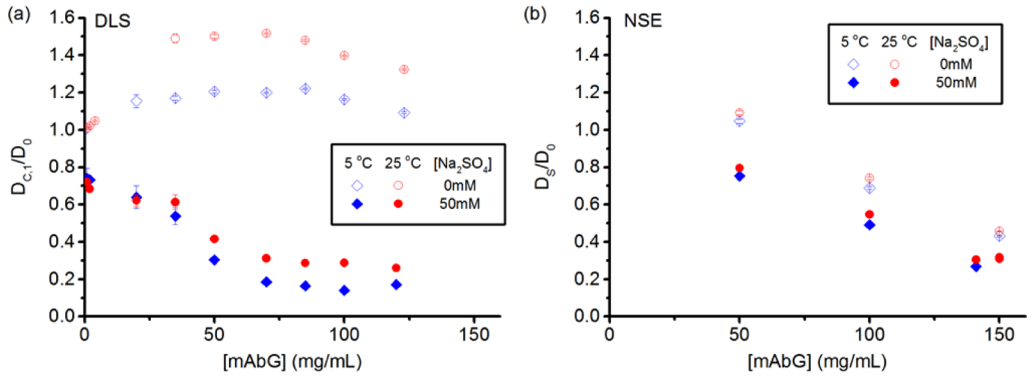


**Figure 5.** (a) Collective diffusion coefficients and (b) short-time self-diffusion coefficients normalized by the bare diffusion of an mAbG monomer, $D_0$, plotted separately on the same scale. Deviations due to the presence of $Na_2SO_4$ are significant for long-time collective motion in panel a, but relatively insignificant for the short-time mobility of individual moving units in panel b.

This 12-bead model provides insight into the antibody structure at low concentration. At 0 mM electrolyte, a model based on a single mAb as the fundamental scattering unit quantitatively fits the SANS spectra. In the case of no added electrolyte, the crystal structure of an IgG1 protein is compared to the best-fit coarse-grained monomer structure in Figure 3b. The two structures are remarkably similar, despite the expectation that configurations might differ between the solid and fluid states.

The scattering profile for mAbG solutions with 50 mM added $Na_2SO_4$ cannot be fit by any single monomer model. Rather, it is well described by scattering from a dimer composed of two mAbG proteins with a conformation similar to that observed for solutions with 0 mM added electrolyte, shown in Figure 3c. Comparison of the scattering intensities from experiment and several model configurations of a monomer and dimer demonstrates the inability of a monomer structure to reproduce the SANS data of samples containing 50 mM $Na_2SO_4$. The insets of Figures S1 and S2 in the SI clearly distinguish $R_g$ values between electrolyte conditions (from the slope) and highlights the sensitivity of the 12-bead model to these differences. This sensitivity provides confidence in the elongated conformation of the dimer extracted from the model fit. Further, the relative sizes of the elongated dimer and monomer from the model quantitatively agree with the static SANS and DLS measurements and are consistent with a previously studied mAb known to form elongated dimers.[15]

Determination of the mAbG conformation in dilute solution is important for understanding the effective structure and dynamics at higher concentrations. Because the dimer takes on an elongated configuration at low protein concentration, the development of large structures and high viscosities are observed at elevated protein concentrations. Already, the effective radii of samples with 50 mM $Na_2SO_4$ increase approximately linearly with mAb concentration up to 10 mg/mL, shown in Figure 2. These trends could be indicative of an increase in cluster size or conformation with increasing protein concentrations. However, in the low-$q$ range, at high enough concentrations, the scattering patterns are also affected by $S(q)$ as a result of mAb−mAb interactions such that it is difficult to directly obtain protein microstructure information quantitatively. Therefore, in the following, we use NSE spectroscopy to study the short-time diffusivity to better understand the moving units at higher concentrations.

**Microstructure of Concentrated Protein Solutions.** Reversible cluster formation at high protein concentrations can be determined by measuring protein dynamics, as previously shown for other mAbs and globular proteins.[15,28] Changes in either electrolyte concentration or temperature directly influence the equilibrium microstructure, both of which have effects on protein mobility. Antibody diffusion is probed by both NSE spectroscopy and DLS, which cover significantly different length and time scales. The correlation functions obtained by both NSE spectroscopy and DLS, with their corresponding best fits using exponential functions, are compared in the SI to highlight the difference in time scales of the extracted collective diffusion coefficients.



DOI: 10.1021/acs.jpcb.5b07260
J. Phys. Chem. B 2016, 120, 278−291

NSE data are obtained for correlation times up to 50 ns, which are then fit to an exponential function to extract the short-time collective diffusion coefficient. A range of $q$ values are studied using NSE spectroscopy, which can demonstrate the change in mobility over a range of length scales. The $q$-dependent short-time collective diffusion coefficients obtained from fits to the NSE data are compiled in Figure 4. Note that, because of the configuration setup in our experiments, we did not measure some $q$ values around 0.2 Å$^{-1}$. The average value of $D_c$ in the limit of large $q$ values was calculated as outlined in a previous work[22] and used to estimate the short-time self-diffusion coefficient, $D_s$. Specifically, values of $D_s$ were estimated at $q$ values above 0.114 Å$^{-1}$, corresponding to sizes on the order of a protein monomer. The decrease of short-time $D_c(q)$ values at smaller $q$ values indicates an influence of structure and hydrodynamics in line with eq 5b, which is discussed in more detail in the SI.

DLS measures the long-time collective diffusion coefficient in protein solutions. Here, the single $q$ value (0.0018 Å$^{-1}$) used in DLS corresponds to a length scale of roughly 350 nm. At low protein concentrations, the data are well fit by a single relaxation mode, whereas a slow mode develops at higher concentrations and requires a double-exponential fit. The subsequent analysis focuses on only the fast mode of long-time collective diffusion, $D_{c,1}$, which is the dominant contribution at all solution conditions (see the discussion in the SI). The exact reason for the slow motion at high concentration is still under investigation. However, it is likely due to the formation of large transient clusters, as further discussed later in relation to the analysis of the rheological data.

Figure 5 shows the values of $D_s$ from NSE analysis and $D_{c,1}$ from DLS normalized by the bare diffusion of an mAbG monomer, $D_0$. Comparison of these results highlights the considerable discrepancy between the short-time mobility of mAbG and the long-time collective motion. In general, the long-time collective diffusivity is a strong function of protein concentration and temperature. As shown in Figure 5a, the mobility in samples without electrolyte is observed to increase initially with increasing concentration. Although this behavior appears to be counterintuitive, this trend is consistent with the theoretical relationship between $D_{c,1}$ and $S(q)$ highlighted in eq 5a. Eventually $D_{c,1}$ reaches a maximum and then decreases at sufficiently large concentrations. This is due to self-crowding and hydrodynamic effects that retard long-time dynamics more significantly than interactions reduce the magnitude of $S(q)$ at small $q$ values,[39] which originally caused the increase in $D_{c,1}$. In contrast, samples with added electrolyte show a rapid decline in $D_{c,1}$ with increasing concentration. Under these conditions, $D_{c,1}$ decreases due to both an increase in low-$q$ scattering and, therefore, $S(q)$ (see eq 5a) and the subsequent reduction in long-time mAb mobility resulting from strong attractive interactions. Hence, the DLS data clearly indicate that, without added salt, the net interaction between mAbG proteins is repulsive, whereas the attractive interaction dominates in the presence of salt. The interaction between mAbG proteins is discussed later in detail in the analysis of SANS data.

For both sets of electrolyte conditions, decreasing temperature reduces long-time protein diffusivity, which is likely a result of enhanced attractive interactions. Despite the prevalence of repulsive interactions in samples without electrolyte, the reduction in $D_{c,1}$ at high concentrations might indicate that mAbG also associates into larger clusters under these conditions. These results are consistent with our rheological results, which are discussed in the following section.

The short-time mobility as probed by NSE spectroscopy probes the fundamental "moving units" in solution by probing motion on the nanoscale on the time scale of up to ∼50 ns. Interestingly, $D_s$ is nearly identical at all concentrations below 50 mg/mL for samples at low ionic strength. This trend was recently observed for another antibody[15] and might be a generic feature of these macromolecules. Previous work demonstrated that the short-time self-diffusion of a charge-stabilized mAb was significantly reduced at high concentrations by hydrodynamic interactions, even though the mAb remained dispersed as monomers.[15] These prior results can be considered representative of the standard dynamic behavior of an mAb monomer. After normalization of the absolute values of $D_s$ with the solvent viscosity, the bare diffusion coefficients are nearly identical between mAbG solutions without electrolyte and these prior results. Therefore, from this comparison, mAbG samples without electrolyte can be considered mostly monomers in the short-time limit at all mAb concentrations studied.

The most substantial impact on $D_s$ comes from the addition of 50 mM $Na_2SO_4$. An effective hydrodynamic radius of mAbG with electrolyte can be estimated by taking the ratio of self-diffusivities as $R_h/R_0 = D_s(0\ \text{mM})/D_s(50\ \text{mM})$. This ratio is indicative of the size of strongly bound clusters in samples with electrolyte relative to an mAbG monomer. The resulting values of this ratio are presented in Figure 6 for results derived from

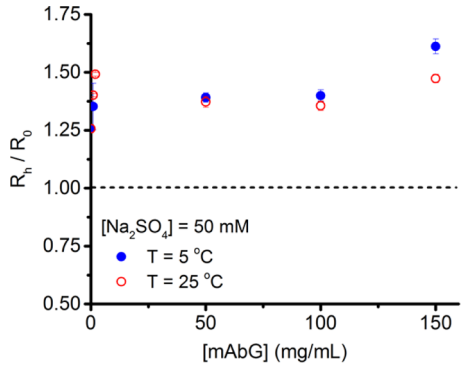


**Figure 6.** Effective hydrodynamic radius of the moving unit with 50 mM $Na_2SO_4$ as a function of temperature and protein concentration.

NSE spectroscopy. The ratio indicates that the relative size of the "fundamental" moving unit for solutions with 50 mM $Na_2SO_4$ remains almost unchanged at all concentrations studied. In other words, at this electrolyte concentration, the mAb always associates into elongated dimers that persist at higher mAb concentrations. The formation of dimers in formulations with 50 mM $Na_2SO_4$ can be also seen from $D_{c,1}/D_0$ shown in Figure 5a as $D_{c,1}/D_0$ values are less than 1 at low protein concentrations. Combining the results for both $D_s$ and $D_{c,1}$, hierarchical cluster formation occurs in the concentrated samples with 50 mM $Na_2SO_4$. The fundamental units are strongly bound dimers with added 50 mM $Na_2SO_4$, which further interact with each other to form transient, larger-scale networks. This is consistent with the rheological data and supported by the strong low-$q$ scattering from SANS data that is discussed later in the article.

The temperature dependence of $D_s$ and $D_{c,1}$ is consistent with a hierarchical association into structures with correlation


DOI: 10.1021/acs.jpcb.5b07260
J. Phys. Chem. B 2016, 120, 278−291

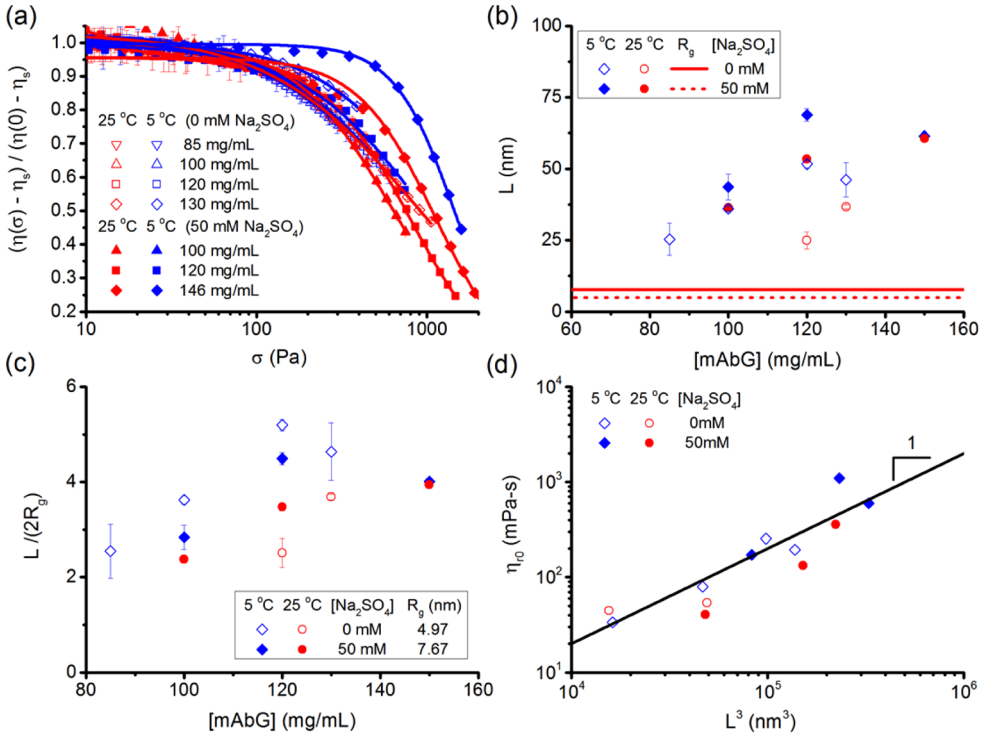


**Figure 7.** (a) Cross model scaling of the viscosity as a function of stress for samples that display shear-thinning behavior. All curves appear nearly identical, indicating that structural deformation is controlled by stress. (b) Characteristic structural length scale at the point of shear thinning. (c) Values of $L$ normalized by the corresponding radius of gyration for each electrolyte condition listed in the legend. (d) Zero-shear viscosity as a function of the cube of the length scale.

lengths much larger than the length of a single antibody. The normalized self-diffusion coefficients shown in Figure 5b are not changed by varying temperature. This indicates that the fundamental moving unit is itself unchanged with temperature for each electrolyte concentration. However, temperature decreases lead to significant decreases in $D_{c,1}$ (as well as increases in viscosity), which indicates a growing correlation length at the longer length and time scales probed by light scattering.

**Shear Thinning and Effective Structure Size of Large Transient Clusters.** Rheological measurements are a sensitive probe of the formation of large-scale structure in solution.[46] The zero-shear viscosity plateau is observed for all solution conditions, but a shear-thinning regime is found to arise at high protein concentrations. The shear rate at which shear thinning occurs decreases with increasing concentration and decreasing temperature. Measurements of the shear-rate-dependent viscosities for all solution conditions studied here are presented in Figure S8 in the SI.

Deviations from Newtonian behavior indicate that the inverse of the shear rate is comparable to a time scale in the material that is representative of structural rearrangement under flow. In particular, the onset of a shear-thinning regime occurs when shear forces become comparable to Brownian forces. The balance of these forces is captured at high concentration by the rescaled Péclet number $Pe = \dot{\gamma}L^2/2D_s$, where $L$ is the characteristic length scale.[47] For these calculations, the shear rate can be replaced by the stress dependence of the viscosity, $\dot{\gamma} = \sigma/\eta(\sigma)$. In these mAb formulations, $L$ can be associated with the representative size of large-scale, transient mAb clusters. Shear thinning generally occurs at $Pe \geq 1$. Therefore, the transition point at $Pe \approx 1$ is indicative of an effective association structural length scale in solution.

Studies of dispersions of colloidal hard-sphere (HS) and charged-sphere (CS) or electrostatically stabilized particles have demonstrated that shear thinning can be accurately modeled with respect to shear stress.[46] When the stress is normalized by a critical value (as a function of volume fraction), the behavior is universal across all systems.[46] The viscosities of all concentrated mAbG formulations displaying shear-thinning behavior are plotted in Figure 7a, normalized according to the Cross model. Here, the solvent viscosity is used to represent the high-shear viscosity, but the results are relatively insensitive to this value. Consistent with expectations from colloid rheology, the mAbG viscosities normalized in this manner show a common behavior as a function of absolute shear stress. The similarity indicates that the breakdown of the association structures of mAbG is stress-dependent ($\sigma$) as opposed to rate-dependent ($\dot{\gamma}$). (In the SI, the onset of shear thinning is shown to differ significantly as a function of shear rate between conditions.) A distinctive outlier is the most viscous solution at highest mAb concentration with added electrolyte at the lowest temperature.

Whereas the critical shear stress is relatively insensitive to the addition of electrolyte (50 mM $Na_2SO_4$), the characteristic length scale estimated from these values varies significantly as a result of the differences in viscosities and short-time self-diffusivities (compare scales of Figure 1 and Figure 5b, respectively). The characteristic length scale, $L$, is estimated by setting $Pe = 1$ and assuming that the critical shear-thinning point occurs at a 50% reduction in the low-shear-rate limiting value.[46] These values of $L$ are plotted in Figure 7b as a function of sample composition.


DOI: 10.1021/acs.jpcb.5b07260
J. Phys. Chem. B 2016, 120, 278−291

For all samples, the characteristic length scale determined from the shear-thinning viscosity is significantly larger than the protein size, which is also shown for reference in Figure 7b. Samples with added electrolyte are found to have larger characteristic length scales than those without added electrolyte at a given temperature and composition. This could be anticipated because of the presence of strongly bound dimers as a larger fundamental moving unit in samples with added electrolyte. When these length scales are normalized by the effective diameter (twice the radius of gyration) of the smallest moving unit under each set of conditions (monomer without electrolyte, dimer with electrolyte), plotted in Figure 7c, the resulting value is an effective association size in solution at the conditions of interest. These sizes appear relatively insensitive to the solution conditions and increase slightly with increasing mAb concentration.

Note that this estimation depends on the choice of the critical shear-thinning point. If the same calculation of $L$ is performed using the point where $\eta$ is only 20% of $\eta_0$, then the length scales become roughly a factor of 3 larger. Nonetheless, the structural units of size $L$, which form from the interaction between fundamental moving units, associate hierarchically into larger dynamically correlated structures.

In the short-time limit, monomers in samples without added electrolyte and dimers in samples with added electrolyte move freely on the nanometer length scale. However, associations between proteins at higher concentrations lead to shear-thinning behavior in the bulk. A strong correlation is observed between the solution zero-shear viscosity and mAbG association represented by $L^3$, as shown in Figure 7d. This analysis indicates that the viscosity increases proportionally with the cube of the length scale, as expected for particulate suspensions,[46] as well as for semidilute polymer suspensions.[16]

Combining the analysis of SANS data, rheological data, and NSE and DLS results, we show a schematic representation of the microstructures supported by experimental evidence in Figure 8. The fundamental unit size and subsequent associations are distinguished between the two sets of electrolyte conditions conclusively using NSE spectroscopy. For the samples without added salt, NSE spectroscopy shows that the proteins move as individual molecules on nanosecond and nanometer scales, whereas the bulk rheology and DLS results suggest associations on longer length and time scales. However, in the presence of 50 mM $Na_2SO_4$, strongly bound dimers form already at relatively low concentrations and remain as the moving units at high concentrations. The rheological data indicate that these dimers form loosely bound large clusters.

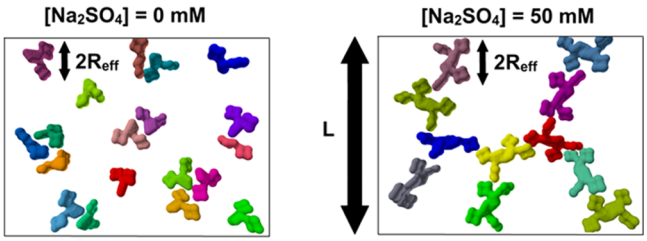


**Figure 8.** Schematic of proposed solution microstructures with corresponding fundamental moving units over short time and length scales ($2R_{eff}$) compared under conditions of 0 and 50 mM added electrolyte . Without added $Na_2SO_4$, structures contain a dispersion of monomers and dynamic clusters (composed of monomers). With 50 mM $Na_2SO_4$, transient networks form with a characteristic length scale ($L$) due to weak association of long-lived dimers.

**Effective mAb−mAb Interactions and Their Impact on Solution Microstructure.** SANS experiments were performed on mAbG solutions to gain some physical insight into the protein−protein interactions that mediate the solution microstructure and bulk properties such as viscosity. SANS scattering intensities of mAbG formulations at several protein concentrations are shown in panels a and b of Figure 9 for samples with 0 and 50 mM added $Na_2SO_4$, respectively. The increase in high-$q$ scattering intensity with increasing protein concentration is due to the corresponding increase in hydrogen content, which contributes to the background due to strong incoherent scattering.

For solutions without added electrolyte, increasing protein concentration leads to the development of a structure peak in the scattering evident as a maximum in the overall scattering intensity. The "correlation hole" at low $q$ evidenced by the reduction in the forward scattering corresponds to a decrease in osmotic compressibility typical for concentrated systems with strong repulsive interactions.[48] This is clearly demonstrated by the low-$q$ region of the structure factor, shown in Figure 9c for these samples. Furthermore, $I(q)$ and $S(q)$ of samples without electrolyte are nearly independent of temperature. These trends are consistent with screened electrostatic repulsion that is relatively temperature-insensitive.

A comparison of samples with 0 and 50 mM $Na_2SO_4$ at equivalent mAb concentration clearly shows a strong increase in low-$q$ scattering upon electrolyte addition, which signifies a change in mAb−mAb interactions. The addition of 50 mM $Na_2SO_4$ significantly enhances the low-$q$ scattering by roughly an order of magnitude at concentrations above 50 mg/mL. This large increase in intensity indicates the dominance of strong interprotein attractions, which is reflected in $S(q)$, shown in Figure 9d. The substantial scattering intensity at small $q$ values observed in formulations with 50 mM $Na_2SO_4$ suggests the presence of longer-scale structural features, which are consistent with the large loosely bound clusters indicated by the rheological results and DLS data. Furthermore, unlike the case for mAbG solutions without added electrolyte, changing temperature results in noticeable increases in the scattering pattern of mAbG solutions with 50 mM $Na_2SO_4$. At 5 °C, the intensity at low $q$ is nearly double that measured at 25 °C, indicating that the attractions are stronger at lower temperature. Such a strong temperature dependence suggests that hydrophobic interactions play an important role in determining the strength of attraction, as observed previously.[49]

To understand the effective interprotein interaction, $S_{eff}(q)$ was extracted according to eq 1 using SANS data and is shown in Figure 9. Theoretical structure factors, $S(q)$, were calculated using integral equation theory with the model HSDY potential, eq 4. Using the 12-bead model form factor fits derived from dilute solution, $\beta(q)$ was estimated to calculate $S_{eff}(q)$ from $S(q)$. The best fits using the theoretically calculated $S_{eff}(q)$ are shown in Figure 9c,d as lines through the data. All resulting fit parameters are tabulated in the SI. The corresponding potentials derived from fitting the SANS data are shown in Figure 10 and interpreted as follows. Note that understanding protein−protein interaction is very challenging. If the detailed protein structure is available, there are different methods for estimating the protein−protein interactions.[50] However, without those details, qualitative information on the effective


DOI: 10.1021/acs.jpcb.5b07260
J. Phys. Chem. B 2016, 120, 278−291

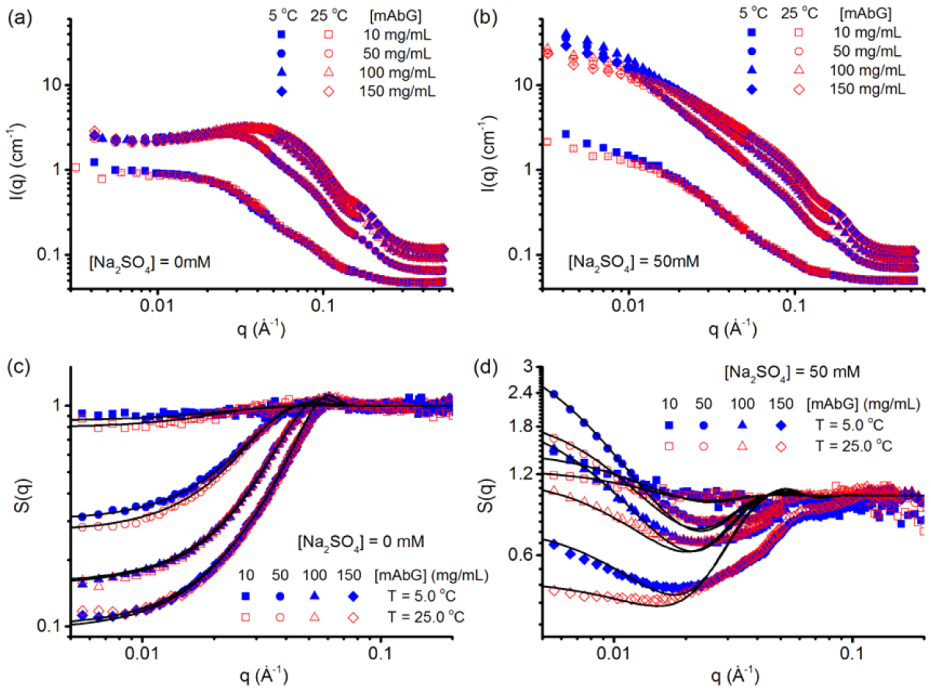


**Figure 9.** (a,b) Reduced one-dimensional scattering profiles for several mAbG concentrations with (a) 0 and (b) 50 mM added $Na_2SO_4$ electrolyte at 5 and 25 °C. (c,d) Structure factors for the same mAbG concentrations with (c) 0 and (d) 50 mM added $Na_2SO_4$ with $S(q)$ fits (lines) using the HSDY potential and corresponding $\beta(q)$ functions.

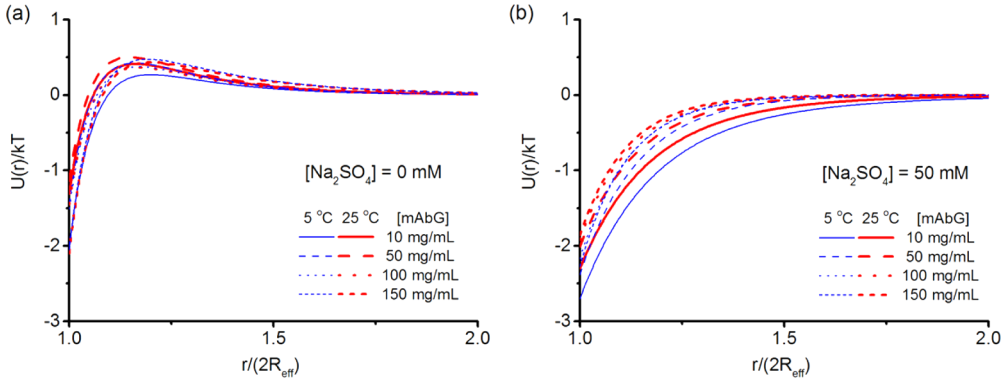


**Figure 10.** Potentials extracted from fits to the SANS data using the 12-bead model for samples with (a) 0 and (b) 50 mM $Na_2SO_4$. Antibodies interact with an effective attraction in the presence of added $Na_2SO_4$, which screens the weak, long-range repulsion found in samples without added electrolyte.

protein−protein interactions can still be extracted from the SANS data.[14]

For samples without added $Na_2SO_4$, the data are fit very well using the monomer form factor with a combination of competing interactions of reasonable magnitude. Indeed, the potentials resulting from best fits to the SANS profiles contain a short-range attraction between mAbG proteins in addition to long-range electrostatic repulsion. The structure factors show the correlation hole typical of colloidal dispersions interacting with long-range repulsions,[51] but without the characteristic structure peak.

We caution that this interpretation is based on a spherically symmetric potential acting between anisotropic mAb proteins, which probably have anisotropic interactions. The small strength of attraction determined from these fits could result from an abundance of weakly interacting orientations, whereas a few specific configurations of two closely separated monomers could produce very strong attractive forces. This possibility is supported by recent work on this antibody, which demonstrates an acute sensitivity of association to the inclusion of specific surface residues in the IgG1 structure.[52] An atomistic or coarse-grained simulation[29] would be required to more accurately model these anisotropic interactions and is beyond the scope of this work, but the spherically averaged potential already yields valuable insight into the microscopic structure of these concentrated mAb solutions.

Structure-factor fitting with a spherically symmetric potential was found to be less satisfactory for samples with 50 mM $Na_2SO_4$. Note that the obtained interaction potential is that between strongly bound dimers (as the fundamental moving units). Figure 9d shows that the important long-range structure at low $q$ values can be accurately captured, whereas the intermediate $q$ range is poorly fit, especially at higher concentrations. Because dimers are the dominant moving unit, the mAb structure model was implemented by taking a dimer as the form factor in the SANS fitting. Despite this


DOI: 10.1021/acs.jpcb.5b07260
J. Phys. Chem. B 2016, 120, 278−291

inability to quantitatively model the intermediate $q$ range, the fitting results are still qualitatively useful as the satisfactory fitting for the low-$q$ regime is the most sensitive to effective interprotein interactions. The fits yield a spherically symmetric potential of interaction with a significant primary attractive well and no stabilizing long-range repulsion, as shown in Figure 10b. This is consistent with the significant increase in scattering intensity observed in the SANS profiles for samples with added electrolyte shown in Figure 9b. The nearly identical potentials determined independently from the scattering for all mAbG concentrations is consistent with the results from the NSE data that dimers are the fundamental moving and interacting unit at all concentrations and both temperatures. It is noted that the decoupling approximation was used in the fitting, which assumes that the interparticle distance is independent of the orientation/conformations of individual particles.[32,33] This assumption is questionable especially when mAbs are in close proximity, such that the dimer association structure might depend on the solution concentration. However, this does not affect the conclusions that the interaction between the strongly bound dimers is dominated by an attraction.

This detailed analysis of the SANS data qualitatively reveals the physical mechanism for the formation of larger association structures that increase the zero-shear viscosity. The size of the fundamental unit and subsequent associations are distinguished between the two electrolyte conditions, consistent with the results from the NSE data. The presence of competing forces in samples without added electrolyte demonstrates that mAbG monomers can reversibly associate into large transient clusters. NSE spectroscopy shows that the proteins move as individual molecules on nanosecond and nanometer scales, whereas the bulk rheology and diffusion measurements suggest associations on longer length and time scales. Similarly, the interactions between dimers in the presence of 50 mM $Na_2SO_4$ indicate a strong driving force to associate dimers into large-scale, loosely bound transient clusters. If dimers do associate by their $F_c$ domains, leaving hydrophobic CDR regions exposed in extended structures,[49] the presence of multiple physical interaction points on a single dimer would have the potential to form large network structures in concentrated solutions.[13,29] Again, the NSE data suggest that the fundamental unit for samples with added electrolyte is a dimer.

**Microscopic Contributions to Viscosity Based on Existing Models.** In this section, a micromechanical viscosity model is used to qualitatively validate the importance of microscopic forces leading to the differences in zero-shear viscosity as a function of solution conditions. Further, we test the ability of recently proposed viscosity models to independently identify the same structural and dynamic properties as extracted by analyzing neutron scattering data.

Theoretical descriptions of the relative zero-shear viscosity of colloidal suspensions include contributions from hydrodynamic ($\eta_H$), Brownian ($\eta_B$), and interaction ($\eta_I$) components, such that $\eta_{r0} = \eta_H + \eta_B + \eta_I$.[53,54] The hydrodynamic contribution is obtained experimentally and compared with established relationships,[54] which is shown to be a relatively small component of the solution viscosity (more details can be found in the SI). Therefore, the focus of this analysis is to use the extensive data measured in this work to isolate the contribution of the interparticle interactions to the viscosity and compare this contribution with the structural analysis presented above. The hydrodynamic contribution is combined with the Brownian and attractive interaction terms, which are determined from a theory for spherically symmetric interactions in the limit of hydrodynamic preaveraging as

$$\eta_{r0} = \left(\eta_H + \frac{12}{5}\frac{\phi^2 g(2)}{D_s/D_0}\right)\left(1 + 1.9\frac{\phi^2}{\tau_B}\right) - 2\int_{r_{max}}^{\infty} g(r')\frac{dU_{rep}(r')}{dr}\,dr' \quad (7)$$

where $r_{max}$ is the separation at the energy maximum in the HSDY potential. The volume fraction $\phi = (C/M_w)(4\pi R_h^3/3)$ was calculated using the $M_w$ and $R_h$ values determined from SANS and DLS, respectively, of the fundamental mAbG moving unit. Note that the values of $R_g$ determined from SANS and $R_h$ determined from DLS and hydrodynamic modeling are all consistent and interchangeable with little difference in the final value. All of the parameters in this equation are known from our analysis of the NSE data (yielding $D_s/D_0$ from Figure 5b); the effective spherically symmetric interaction potential, $U(r)$, shown in Figure 10; and the corresponding pair distribution function, $g(r)$. The contribution from attractive interactions can be captured by a previously developed relationship[55] with the Baxter parameter, $\tau_B = 0.25/(1 - B_2^*)$, where $B_2^*$ is the second virial coefficient normalized by a HS fluid at the same volume fraction. Here, $\tau_B$ is determined from only the attractive portion of each potential shown in Figure 10, leaving only the long-range repulsive component of the potential in the final integral.

Figure 1 shows the experimental solution viscosity relative to the range of estimated viscosities for a HS fluid (gray region) and the estimates using eq 7 from mAb structural and dynamic data (blue-red region). The wide range of values reflects the uncertainty in these calculations as well as the range of solution conditions represented. Within the HSDY region, the upper blue portion reflects estimates from samples at 5 °C, whereas the lower red region is representative of samples at 25 °C. Although capturing many qualitative aspects of the variation with solution conditions, the predictions for $\eta_{r0}$ fall well below the experimental viscosities. Predictions of the viscosity require accurate predictions or measurements of the structure and forces, such that the isotropic potentials derived from fitting the SANS data cannot be expected to be very accurate. This analysis suggests that an analysis that explicitly treats the anisotropic interaction potential between mAbs and mAb dimers would improve the viscosity predictions.

We also briefly consider a recent model proposed for the zero-shear viscosity of associating mAb solutions based on polymer network theory.[56] The zero-shear viscosity of mAbG is fit using the antibody network model,[56] shown in the SI, which has the following functional form

$$\eta_0 = Ac^{3/(3\nu-1)}\left[\frac{2kc}{\sqrt{1+4kc}-1}\right]^3 \quad (8)$$

where $A$ is a constant, $c$ is the protein concentration in mg/mL, $\nu \approx 0.6$, $k$ is the partition function between all possible association states, and the term in the square brackets is the aggregation number, $\langle N\rangle$. Note that the model is based on long, entangled polymer-like aggregates[56] and is therefore expected to be accurate only at high concentrations. Whereas the derived parameters are very sensitive to the range of data fit by eq 8, they are expected to be representative of the solution


DOI: 10.1021/acs.jpcb.5b07260
J. Phys. Chem. B 2016, 120, 278−291

structure under those conditions. Here, viscosity data for only the highest three mAbG concentrations are used.

The model fits can be interpreted in terms of a characteristic chain length as $3b\langle N\rangle$, where $3b$ is the longest dimension of an individual antibody, shown previously for mAbG to be about 15 nm.[30] The effective aggregate lengths extracted from the model fitting, shown in the SI, agree semiquantitatively with the effective length scales obtained from the shear-thinning behavior of the viscosity observed at similar protein concentrations. However, as pointed out in the original article by the authors, the model is based on long, entangled polymer-like aggregates,[56] raising concern as to the accuracy of the small aggregate sizes extracted from the model. Further, the fact that these aggregates are composed of dimers in mAbG samples with 50 mM added $Na_2SO_4$ cannot be deduced from this model fitting.

Trends in the viscosity of concentrated mAb solutions have also been modeled by the modified Ross–Minton equation[13]

$$\eta_{r0} = \exp\left[\frac{[\eta]c}{1 - (k/\nu)[\eta]c}\right] \tag{9}$$

where $[\eta]$ is the intrinsic viscosity; $c$ is the protein concentration in g/mL; and $k/\nu$ is an association term composed of the Simha shape parameter, $\nu$, and a self-crowding factor, $k$.[13] The self-crowding factor is proportional to the interaction strength and inversely proportional to the maximum packing fraction. Similarly, the Simha shape factor can be regarded as an effective association structure size.

The Ross–Minton model describes the concentration dependence of solution viscosity based on the assumption that the parameters $[\eta]$ and $k/\nu$ are constant. However, nonlinearity in the data when plotting $\ln(\eta_{r0})/c$ as a function of $\ln(\eta_{r0})$, as shown in the SI, indicates that both model parameters are functions of protein concentration. For example, a change in aggregate size is expected to simultaneously alter the intrinsic viscosity and the Simha shape parameter. Therefore, without additional information, this model is unable to distinguish the contributions of solution structure and mAb–mAb interactions to the solution viscosity.

Previous studies of antibody viscosity behavior using the Ross–Minton model have relied on the extrapolation of linear fits to (nonlinear) high-concentration data to the dilute limit to extract an effective intrinsic viscosity.[10,13] The typically larger magnitude of $[\eta]$ determined in this manner relative to that at low concentrations has been used to hypothesize that large aggregates have formed in concentrated solutions. However, as discussed in the SI for solutions of mAbG, a change in the slope of a Ross–Minton plot (i.e., the apparent magnitude of $k/\nu$) suggests that solutions have either larger aggregates, weaker associations, or both. Through a collective analysis of the SANS, NSE, and rheology results, the viscosity of solutions with no added electrolyte was identified to be the result of smaller aggregates that interact by a weak attraction and a strong repulsion, in contrast to solutions with 50 mM added electrolyte, for which the viscosity results from large clusters formed by only a weak attraction. Note that the modified Ross–Minton model is unable to distinguish between attractive or repulsive interactions or the size of the fundamental unit of which aggregates are composed. Such conclusions require the additional knowledge afforded by the analysis of neutron scattering data.

Quantitatively distinguishing the influence of formulation composition (such as added electrolyte) on effective interactions provides additional insight into the nanoscale interactions and structures resulting in the solution viscosity behavior. Previously, large viscosities in solutions of mAbG and other antibodies at high concentration have been qualitatively related to an effective cluster size.[13,15,16] However, cluster interactions have been discussed as an additional important contribution to the viscosity. The importance of interprotein interactions under shear is consistent with prior work on mAbG by Lilyestrom et al.[13] Therefore, this work complements prior research by identifying the fundamental diffusing unit as being dimers in the presence of added electrolyte and by showing that the association of clusters forming at higher concentration arises from different interprotein interactions depending on the electrolyte concentration. Furthermore, this new knowledge helps to semiquantitatively explain the significant rise in viscosity with increasing mAb concentration, electrolyte addition, and reduced temperature.

Interestingly, the viscosity of mAbG that forms large transient clusters in the presence of electrolyte is similar to the viscosity of a previously studied mAb that was reported to form small long-lived clusters at 25 °C.[15] These small clusters were demonstrated to be elongated structures, similar to mAbG with electrolyte. Particles with larger aspect ratios are known to produce higher viscosities, which, combined with electrostatic repulsion, was highlighted previously as the cause for the observed viscosity.[15] Here, the viscosity of mAbG with added $Na_2SO_4$ appears to be driven primarily by attractive interactions. These forces cause protein dimers to associate into a distribution of cluster sizes that collectively resist shear flow. However, mAbG dimers remain mobile and exchange between local environments to maintain fluidity. Therefore, the existence of a universal correlation between average cluster size and viscosity is questionable. Rather, the extent of dimer/cluster formation, cluster size/shape, and effective cluster–cluster interactions will dictate the viscosity. Consequently, these characteristics can lead to dramatically different solution microstructures, yet still produce similar macroscopic solution properties.

It is important to recognize the significance of the short-time dynamics in systems such as mAbG, where proteins are one component/species of a highly polydisperse dynamic microstructure. NSE data indicate that the fundamental mAbG moving units remain mobile in the short-time limit. However, depending on the effective interactions, the fundamental units can associate into larger transient clusters, which will be strongly influenced by the morphology of the strongly bound small clusters. How this hierarchical cluster formation quantitatively leads to the zero-shear viscosity requires further investigation.

## ■ CONCLUSIONS

The experimental evidence presented throughout this work in combination with previous studies[13,30] indicates that mAbG, a relatively hydrophobic IgG1 antibody, can reversibly associate into loosely connected clusters in the absence of added $Na_2SO_4$ salt. These large clusters are composed of monomers as small moving units at the short-time limit. However, in the presence of 50 mM $Na_2SO_4$, mAbG proteins form dimers that are long-lived and have an elongated conformation. These dimers associate hierarchically into large, loosely bound transient clusters at higher mAb concentrations, whose fundamental


DOI: 10.1021/acs.jpcb.5b07260
J. Phys. Chem. B 2016, 120, 278–291

moving unit at the short-time limit are these dimers. The large transient clusters formed by the interacting dimers cause a significant increase of the viscosity when the salt is added. Even though the viscosity of the mAb studied in this article depends on the salt concentration in a completely different way than observed in a previously studied case,[15] we found that the microscopic structural origins are surprisingly similar. In both cases, mAb proteins can form dimers as fundamental units. This finding also seems to indicate that the formation of extended dimers might be a common feature of mAb solutions exhibiting higher viscosities besides the two cases studied here. Their effective interactions play a significant role in the resulting macromolecular structure and viscosity.

Several existing viscosity models were shown to provide useful, semiquantitative information concerning the underlying microstructure in viscous mAb solutions, especially when combined with structural and dynamic experiments. The accurate modeling of the viscosity of concentrated protein solutions still requires more thorough characterization of cluster properties. Although the existence of a universal relation between cluster formation and viscosity remains elusive, characterization of the appropriate properties can still aid in the optimization of biopharmaceutical therapeutic formulation.

## ■ ASSOCIATED CONTENT

### Supporting Information

The Supporting Information is available free of charge on the ACS Publications website at DOI: 10.1021/acs.jpcb.5b07260.

Detailed development and discussion of the coarse-grained model of a monoclonal antibody using 12 representative spheres (PDF)

## ■ AUTHOR INFORMATION


### Corresponding Authors

*E-mail: zarraga.isidro@gene.com. Phone: 650-225-7617.

*E-mail: yun.liu@nist.gov or yunliu@udel.edu. Phone: 301-975-6235.


### Notes

The authors declare no competing financial interest.

## ■ ACKNOWLEDGMENTS

This manuscript was prepared under cooperative agreements 70NANB12H239 and 70NANB10H256 from NIST, U.S. Department of Commerce. The statements, findings, conclusions, and recommendations are those of the authors and do not necessarily reflect the view of NIST or the U.S. Department of Commerce. The authors also recognize the financial support from Genentech Inc. This work utilized facilities supported in part by the National Science Foundation under Agreement DMR-1508249.

## ■ REFERENCES


(1) Frauenfelder, H.; Sligar, S. G.; Wolynes, P. G. The Energy Landscapes and Motions of Proteins. *Science* **1991**, *254*, 1598−1603.

(2) Bryngelson, J. D.; Onuchic, J. N.; Socci, N. D.; Wolynes, P. G. Funnels, Pathways, and the Energy Landscape of Protein Folding: A Synthesis. *Proteins: Struct., Funct., Genet.* **1995**, *21*, 167−195.

(3) Dill, K. A.; Chan, H. S. From Levinthal to Pathways to Funnels. *Nat. Struct. Biol.* **1997**, *4*, 10−19.

(4) Onuchic, J. N.; Luthey-Schulten, Z.; Wolynes, P. G. Theory of Protein Folding: The Energy Landscape Perspective. *Annu. Rev. Phys. Chem.* **1997**, *48*, 545−600.

(5) Roberts, C. J. Non-Native Protein Aggregation Kinetics. *Biotechnol. Bioeng.* **2007**, *98*, 927−938.

(6) Ross, C. A.; Poirier, M. A. Protein Aggregation and Neurodegenerative Disease. *Nat. Med.* **2004**, *10*, S10−S17.

(7) Rosenberg, A. S. Effects of Protein Aggregates: An Immunologic Perspective. *AAPS J.* **2006**, *8*, E501−E507.

(8) Harris, R. J.; Shire, S. J.; Winter, C. Commercial Manufacturing Scale Formulation and Analytical Characterization of Therapeutic Recombinant Antibodies. *Drug Dev. Res.* **2004**, *61*, 137−154.

(9) Shire, S. J. Formulation and Manufacturability of Biologics. *Curr. Opin. Biotechnol.* **2009**, *20*, 708−714.

(10) Yadav, S.; Shire, S. J.; Kalonia, D. S. Factors Affecting the Viscosity in High Concentration Solutions of Different Monoclonal Antibodies. *J. Pharm. Sci.* **2010**, *99*, 4812−4829.

(11) Yadav, S.; Sreedhara, A.; Kanai, S.; Liu, J.; Lien, S.; Lowman, H.; Kalonia, D. S.; Shire, S. J. Establishing a Link between Amino Acid Sequences and Self-Associating and Viscoelastic Behavior of Two Closely Related Monoclonal Antibodies. *Pharm. Res.* **2011**, *28*, 1750−1764.

(12) Yadav, S.; Laue, T. M.; Kalonia, D. S.; Singh, S. N.; Shire, S. J. The Influence of Charge Distribution on Self-Association and Viscosity Behavior of Monoclonal Antibody Solutions. *Mol. Pharmaceutics* **2012**, *9*, 791−802.

(13) Lilyestrom, W. G.; Yadav, S.; Shire, S. J.; Scherer, T. M. Monoclonal Antibody Self-Association, Cluster Formation, and Rheology at High Concentrations. *J. Phys. Chem. B* **2013**, *117*, 6373−6384.

(14) Yearley, E. J.; Zarraga, I. E.; Shire, S. J.; Scherer, T. M.; Gokarn, Y.; Wagner, N. J.; Liu, Y. Small-Angle Neutron Scattering Characterization of Monoclonal Antibody Conformations and Interactions at High Concentrations. *Biophys. J.* **2013**, *105*, 720−731.

(15) Yearley, E. J.; Godfrin, P. D.; Perevozchikova, T.; Zhang, H.; Falus, P.; Porcar, L.; Nagao, M.; Curtis, J.; Gawande, P.; Taing, R.; et al. Observation of Small Cluster Formation in Concentrated Monoclonal Antibody Solutions and Its Implications to Solution Viscosity. *Biophys. J.* **2014**, *106*, 1763−1770.

(16) Zarraga, I. E.; Taing, R.; Zarzar, J.; Luoma, J.; Hsiung, J.; Patel, A.; Lim, F. J. High Shear Rheology and Anisotropy in Concentrated Solutions of Monoclonal Antibodies. *J. Pharm. Sci.* **2013**, *102*, 2538−2549.

(17) Sciortino, F.; Mossa, S.; Zaccarelli, E.; Tartaglia, P. Equilibrium Cluster Phases and Low-Density Arrested Disordered States: The Role of Short-Range Attraction and Long-Range Repulsion. *Phys. Rev. Lett.* **2004**, *93*, 055701.

(18) Mossa, S.; Sciortino, F.; Tartaglia, P.; Zaccarelli, E. Ground-State Clusters for Short-Range Attractive and Long-Range Repulsive Potentials. *Langmuir* **2004**, *20*, 10756−10763.

(19) Stradner, A.; Sedgwick, H.; Cardinaux, F.; Poon, W. C. K.; Egelhaaf, S. U.; Schurtenberger, P. Equilibrium Cluster Formation in Concentrated Protein Solutions and Colloids. *Nature* **2004**, *432*, 492−495.

(20) Campbell, A.; Anderson, V.; van Duijneveldt, J. S.; Bartlett, P. Dynamical Arrest in Attractive Colloids: The Effect of Long-Range Repulsion. *Phys. Rev. Lett.* **2005**, *94*, 208301.

(21) Klix, C. L.; Royall, C. P.; Tanaka, H. Structural and Dynamical Features of Multiple Metastable Glassy States in a Colloidal System with Competing Interactions. *Phys. Rev. Lett.* **2010**, *104*, 165702.

(22) Porcar, L.; Falus, P.; Chen, W.-R.; Faraone, A.; Fratini, E.; Hong, K.; Baglioni, P.; Liu, Y. Formation of the Dynamic Clusters in Concentrated Lysozyme Protein Solutions. *J. Phys. Chem. Lett.* **2010**, *1*, 126−129.

(23) Liu, Y.; Porcar, L.; Chen, J.; Chen, W.; Falus, P.; Faraone, A.; Fratini, E.; Hong, K.; Baglioni, P. Lysozyme Protein Solution with an Intermediate Range Order Structure. *J. Phys. Chem. B* **2011**, *115*, 7238−7247.

(24) Rosenbaum, D.; Zamora, P.; Zukoski, C. Phase Behavior of Small Attractive Colloidal Particles. *Phys. Rev. Lett.* **1996**, *76*, 150−153.

(25) Chen, S.-H.; Broccio, M.; Liu, Y.; Fratini, E.; Baglioni, P. The Two-Yukawa Model and Its Applications: The Cases of Charged

Proteins and Copolymer Micellar Solutions. *J. Appl. Crystallogr.* **2007**, *40*, s321−s326.
(26) Valadez-Pérez, N. E.; Benavides, A. L.; Schöll-Paschinger, E.; Castañeda-Priego, R. Phase Behavior of Colloids and Proteins in Aqueous Suspensions: Theory and Computer Simulations. *J. Chem. Phys.* **2012**, *137*, 084905.
(27) Cardinaux, F.; Zaccarelli, E.; Stradner, A.; Bucciarelli, S.; Farago, B.; Egelhaaf, S. U.; Sciortino, F.; Schurtenberger, P. Cluster-Driven Dynamical Arrest in Concentrated Lysozyme Solutions. *J. Phys. Chem. B* **2011**, *115*, 7227−7237.
(28) Godfrin, P. D.; Hudson, S. D.; Hong, K.; Porcar, L.; Falus, P.; Wagner, N. J.; Liu, Y. Short-time Glassy Dynamics in Viscous Protein Solutions With Competing Interactions. *Phys. Rev. Lett.* **2015**, *115*, 228302.
(29) Chaudhri, A.; Zarraga, I. E.; Kamerzell, T. J.; Brandt, J. P.; Patapoff, T. W.; Shire, S. J.; Voth, G. A. Coarse-Grained Modeling of the Self-Association of Therapeutic Monoclonal Antibodies. *J. Phys. Chem. B* **2012**, *116*, 8045−8057.
(30) Lilyestrom, W. G.; Shire, S. J.; Scherer, T. M. Influence of the Cosolute Environment on IgG Solution Structure Analyzed by Small-Angle X-Ray Scattering. *J. Phys. Chem. B* **2012**, *116*, 9611−9618.
(31) Scherer, T. M.; Liu, J.; Shire, S. J.; Minton, A. P. Intermolecular Interactions of IgG1Monoclonal Antibodies at High Concentrations Characterized by Light Scattering. *J. Phys. Chem. B* **2010**, *114*, 12948−12957.
(32) Chen, S.-H. Small Angle Neutron Scattering Studies of the Structure and Interaction in Micellar and Microemulsion Systems. *Annu. Rev. Phys. Chem.* **1986**, *37*, 351−399.
(33) Liu, Y.; Chen, W.-R.; Chen, S.-H. Cluster Formation in Two-Yukawa Fluids. *J. Chem. Phys.* **2005**, *122*, 044507.
(34) Zemb, T.; Lindner, P. *Neutrons, X-rays and Light: Scattering Methods Applied to Soft Condensed Matter*; Elsevier B.V.: Amsterdam, 2002.
(35) The MATLAB code for the 12-bead model is available by contacting P. D. Godfrin (godfrin@udel.edu) or Y. Liu (yun.liu@nist.gov).
(36) McQuarrie, D. *Statistical Mechanics*; University Science Books: Sausalito, CA, 2000.
(37) Cardinaux, F.; Stradner, A.; Schurtenberger, P.; Sciortino, F.; Zaccarelli, E. Modeling Equilibrium Clusters in Lysozyme Solutions. *Europhys. Lett.* **2007**, *77*, 48004.
(38) Kim, J. M.; Castañeda-Priego, R.; Liu, Y.; Wagner, N. J. On the Importance of Thermodynamic Self-Consistency for Calculating Clusterlike Pair Correlations in Hard-Core Double Yukawa Fluids. *J. Chem. Phys.* **2011**, *134*, 064904.
(39) Banchio, A. J.; Nägele, G. Short-Time Transport Properties in Dense Suspensions: From Neutral to Charge-Stabilized Colloidal Spheres. *J. Chem. Phys.* **2008**, *128*, 104903.
(40) Nagele, G. On the Dynamics and Structure of Charge-Stabilized Suspensions. *Phys. Rep.* **1996**, *272*, 215−372.
(41) Falus, P.; Porcar, L.; Fratini, E.; Chen, W.-R.; Faraone, A.; Hong, K.; Baglioni, P.; Liu, Y. Distinguishing the Monomer to Cluster Phase Transition in Concentrated Lysozyme Solutions by Studying the Temperature Dependence of the Short-Time Dynamics. *J. Phys.: Condens. Matter* **2012**, *24*, 064114.
(42) Certain commercial equipment, instruments, or materials are identified in this article to foster understanding. Such identification does not imply recommendation or endorsement by the National Institute of Standards and Technology, nor does it imply that the materials or equipment identified are necessarily the best available for the purpose.
(43) Berne, B. J.; Pecora, R. *Dynamic Light Scattering: With Applications to Chemistry, Biology, and Physics*; Dover Publications: Mineol, NY, 2000.
(44) Malfois, M.; Bonneté, F.; Belloni, L.; Tardieu, A. A Model of Attractive Interactions to Account for Fluid−fluid Phase Separation of Protein Solutions. *J. Chem. Phys.* **1996**, *105*, 3290−3300.
(45) Clark, N. J.; Zhang, H.; Krueger, S.; Lee, H. J.; Ketchem, R. R.; Kerwin, B.; Kanapuram, S. R.; Treuheit, M. J.; McAuley, A.; Curtis, J. E. Small-Angle Neutron Scattering Study of a Monoclonal Antibody Using Free-Energy Constraints. *J. Phys. Chem. B* **2013**, *117*, 14029−14038.
(46) Mewis, J.; Wagner, N. J. *Colloidal Suspension Rheology*; Cambridge Series in Chemical Engineering; Cambridge University Press: New York, 2012.
(47) Brady, J. F.; Morris, J. F. Microstructure of Strongly Sheared Suspensions and Its Impact on Rheology and Diffusion. *J. Fluid Mech.* **1997**, *348*, 103−139.
(48) Sandler, S. *An Introduction to Applied Statistical Thermodynamics*; John Wiley and Sons: New York, 2011.
(49) Pindrus, M.; Shire, S. J.; Kelley, R. F.; Demeule, B.; Wong, R.; Xu, Y.; Yadav, S. Solubility Challenges in High Concentration Monoclonal Antibody Formulations: Relationship with Amino Acid Sequence and Intermolecular Interactions. *Mol. Pharmaceutics* **2015**, *12*, 3896−3907.
(50) Kundrotas, P. J.; Alexov, E. Electrostatic Properties of Protein-Protein Complexes. *Biophys. J.* **2006**, *91*, 1724−1736.
(51) Wagner, N. J.; Krause, R.; Rennie, A. R.; D'Aguanno, B.; Goodwin, J. The Microstructure of Polydisperse, Charged Colloidal Suspensions by Light and Neutron Scattering. *J. Chem. Phys.* **1991**, *95*, 494−508.
(52) Scherer, T. M. Cosolute Effects on the Chemical Potential and Interactions of an IgG1Monoclonal Antibody at High Concentrations. *J. Phys. Chem. B* **2013**, *117*, 2254−2266.
(53) Brady, J. F. The Rheological Behavior of Concentrated Colloidal Dispersions. *J. Chem. Phys.* **1993**, *99*, 567−581.
(54) Lionberger, R. A.; Russel, W. B. A Smoluchowski Theory with Simple Approximations for Hydrodynamic Interactions in Concentrated Dispersions. *J. Rheol.* **1997**, *41*, 399−425.
(55) Krishnamurthy, L.-N.; Wagner, N. J. The Influence of Weak Attractive Forces on the Microstructure and Rheology of Colloidal Dispersions. *J. Rheol.* **2005**, *49*, 475−499.
(56) Schmit, J. D.; He, F.; Mishra, S.; Ketchem, R. R.; Woods, C. E.; Kerwin, B. a. Entanglement Model of Antibody Viscosity. *J. Phys. Chem. B* **2014**, *118*, 5044−5049.


DOI: 10.1021/acs.jpcb.5b07260
*J. Phys. Chem. B* 2016, 120, 278−291